Oncology Research, Vol. 15, pp. 169–182
Printed in the USA.

0965-0407/05 $20.00 + .00

www.cognizantcommunication.com

Tumor Transition Zone: A Putative New Morphological and Functional Hallmark of Tumor Aggressiveness

Oscar D. Bustuoabad,*[1] Raúl A. Ruggiero,*[1] Pedro di Gianni,* M. Gabriela Lombardi,* Carolina Belli,* Gabriela V. Camerano,* Graciela Dran,* Carolina Schere-Levy,* Héctor Costa,* Martín A. Isturiz,* Marina Narvaitz,* Nico van Rooijen,‡ Victoria de los A. Bustuoabad,* and Roberto P. Meiss†

*División Medicina Experimental, Instituto de Investigaciones Hematológicas, Academia Nacional de Medicina, Pacheco de Melo 3081, 1425 Buenos Aires, Argentina
†Departamento de Patología, Centro de Estudios Oncológicos, Academia Nacional de Medicina, Pacheco de Melo 3081, 1425 Buenos Aires, Argentina
‡Department of Cell Biology and Immunology, Faculty of Medicine, Vrije Universiteit, Amsterdam, The Netherlands

(Submitted July 12, 2004; revision received December 3, 2004; accepted January 20, 2005)

A small primary or secondary tumor load can occasionally induce more deleterious effects than a histologically identical larger one. In the four murine models studied herein this enhanced tumor aggressiveness could not be attributed to *NRAS* mutations or other hereditary changes, differential vascularization of live tumor tissues, or necrosis content. Instead, the main tumor feature associated with a more aggressive behavior was the presence of a high number of vessels, sometimes filled with inflammatory cells, inside a tumor area, which we have identified and designated as the transition zone between the live and the necrotic zones. Our experiments suggest that during tumor growth, different cachectic factors are produced within the transition and necrotic zones by dying tumor cells and by tumor infiltrating macrophages only reaching the general circulation through the vessels present in the transition zone. Therefore, a small tumor displaying high vascularization of its transition area could be harmful to its host, while, in contrast, a large tumor could behave as a relatively benign one if its transition zone exhibited little or no vascularization, and in consequence its cachectic factors remained "trapped." Similar histological images to those observed in mice were seen in a significant percentage of human cancer biopsies, raising the possibility that such images might have a prognostic value.

Key words: Tumor transition zone; Vascularization; Inflammation; Tumor aggressiveness

The grading and staging of a malignant neoplasm based on its degree of anaplasia, lack of differentiation, tumor size, and spreading have been classified by UICC and AJCC (1–3). Although these parameters are, at present, the best guide for clinical prognosis and treatment, the outcome of malignant diseases cannot always be predicted accurately (4). In addition, cachectic symptoms that may represent significant clinical problems and may account for between 10% and 22% of all cancer death cannot readily be explained either by the local or distant spread of the tumor or by effects of hormones indigenous to the tissue from which the tumor arose (5). The above considerations suggest that up-to-date the mechanisms underlying tumor aggressiveness have not been fully understood. In this article, in order to explore the nature of this phenomenon, we evaluated, using four murine tumors, the putative relationship between a more aggressive tumor behavior and a) the primary and secondary tumor load; b) the existence of *NRAS* mutations in the more aggressive variants of the tumors, on the basis of the claim that missense mutations in NRAS are frequently found in aggressive murine sarcomas and fibrosarcomas and that wild-type NRAS (different from other tumor suppressor genes that only inhibit neoplastic features in cells bearing its oncogenic allele) can suppress or reduce malignant properties of murine tumor cells even in the absence of its oncogene allele, suggesting that NRAS mutations could act as a general enhancer of the transformed phenotype (6); c) the amount of tumor necrosis, the vascularization of different tumor areas, and the type of inflammatory host cells infiltrating the tumor mass (7,8); and d) the presence of TNF-α, IL-1β, and IL-6 cytokines inside the tumor and in the serum of tumor-bearing mice (9–11).

[1]These two authors contributed equally to this work.
Address correspondence to Roberto P. Meiss, Departamento de Patología, Centro de Estudios Oncológicos, Academia Nacional de Medicina, Pacheco de Melo 3081, 5to. piso, 1425, Buenos Aires, Argentina. Tel/Fax: 54-11-4805-8176; E-mail: patologia@oncologia.anm.edu.ar

In addition, we have studied human tumor slides from our files to investigate whether the histological images observed in our murine tumors could also be present in human malignant tumors.

MATERIALS AND METHODS

Animals

BALB/c mice of both sexes and 2–4 months old, weighing 20–22 g, were used throughout. They were raised in our own colony and maintained on Cooperation pellets (San Nicolás, Buenos Aires, Argentina) and water ad libitum. Animals were sex and age matched within each experiment. Experiments were carried out at the Academia Nacional de Medicina de Buenos Aires where there were suitable conditions both for the housing and welfare of the mice. Care for the animals was maintained according to the policies of Academia Nacional de Medicina (NIH Guide and Use of Laboratory Animals).

Murine Tumors

2P-2. A weakly immunogenic T-lymphoma that arose spontaneously in a BALB/c female, 2P-2 is a tumor of small and large cells that display a mature phenotype expressing TdT−, CD4+, CD8+, and CD1− receptors. The tumor grows expansively and can infiltrate the surrounding tissues and regional lymph nodes but without inducing gross hematological alterations. It was maintained by syngeneic SC transplantation and used between passages 3 and 5. Taking into account the Working Formulation and REAL (Revised European-American Classification of Lymphoid Neoplasms) classification, 2P-2 could be a mouse model for a human peripheral T-cell lymphoma, unspecified (12).

C7HI. This is a highly lung metastatic mammary ductal adenocarcinoma that originated in a BALB/c female treated with 40 mg of medroxyprogesterone acetate (MPA) every 3 months for 1 year (13). It is a slow growing and nonimmunogenic tumor that was maintained by syngeneic SC transplantation and used between passages 25 and 27.

MC-C. Fibrosarcoma induced in a 5-month-old BALB/c male 3 months after the SC implantation of a methylcholanthrene pellet. It is a strongly immunogenic tumor that was maintained by syngeneic SC transplantation and used between passages 20 and 25. More detailed description of this tumor is given elsewhere (14).

S-180. Malignant tumor with sarcomatous histological aspect supplied originally from a Rockland mouse. In our laboratory this tumor could be adapted to grow in 100% of BALB/c mice. It is a fast growing and weakly immunogenic tumor that was maintained by SC transplantation in BALB/c mice and used between passages 80 and 86.

Tumor volume was calculated according to the formula of Attia and Weiss (15): tumor volume = $0.4(ab^2)$, where a and b were the longer and smaller diameters, respectively. Tumor weight was measured in an electronic Mettler H-98 scale.

For the maximum tumor burden used in this study, we followed the suggestions of Tisdale (16), which considered tumor burdens used by Tanaka et al. (17) as adequate for cachectic studies.

Human Tumors

Samples of 80 human malignant tumors of different histological type were macroscopically and microscopically analyzed at the Centro de Estudios Oncólogicos, Academia Nacional de Medicina, Hospital Italiano, and Hospital Argerich of Buenos Aires, Argentina. The list of tumors included: carcinoma of colorectum ($n = 13$), breast ($n = 8$), lung ($n = 6$), urinary tract ($n = 7$), male and female genital tract ($n = 7$), skin ($n = 6$), prostate ($n = 5$), thyroid ($n = 3$), pancreas ($n = 3$), oral cavity ($n = 2$), stomach ($n = 2$), liver ($n = 1$), appendix ($n = 1$) and gallbladder ($n = 1$), osteogenic sarcoma ($n = 4$), rhabdomyosarcoma ($n = 3$), glioblastoma ($n = 3$), schwannoma ($n = 2$), malignant meningioma ($n = 1$), anaplastic astrocytoma ($n = 1$) and non-Hodgkin lymphoma ($n = 1$).

Clinical Evaluation of the Health Condition of Tumor-Bearing Mice

The health condition of mice was evaluated and classified through the general objective exam (GOE) used in veterinary medicine by taking into account the state of the fur (skin and hair), nutrition, mobility, and sensory (18). The states were graded as: good: G (similar state to that of control mice without tumors), fair: F (incipient signals of health impairment), bad: B (bristling hair, weight loss up to 20% of the body weight at the start of the experiment, reduced mobility, dyspnea without cyanosis). More careful analysis revealed that bad health condition was invariably associated to catabolism of host body compartments, particularly muscle and adipose tissues. In our previous experience, death of tumor-bearing mice usually occurred 7–12 days after bad health condition was attained.

Surgical Procedures and Histological Studies

In all cases, surgical procedures were carried out under anesthesia using pentobarbitone sodium. Tumors were removed and fixed in 10% formaldehyde phosphate-buffered saline at pH 7 and included in Leica his-

towax paraffin, blended with polymer additives. Serial sections (3–5 μm) were obtained and stained with hematoxylin and eosin and periodic acid-Schiff (PAS).

Necrotic areas could be histologically distinguished from areas of live tissue and quantified following the method of point-counting (19). Grade of poly- and mononuclear infiltration was determined according to Mancini et al. (20).

To quantify the vascularization of tumor tissues, photographs were projected on a screen and vessel density in areas of 0.4 mm diameter was evaluated. Immunostaining was performed by using anti-CD31 endothelial cells (Dako GA, Carpinteria, CA, USA).

Evaluation of Metastatic Foci

Mice were anesthetized with ether and sacrificed by cervical dislocation. The lungs were removed and rinsed in isotonic saline solution and surface metastatic nodules (diameter ≥ 0.1 mm) were counted under a dissecting microscope. The lungs were then processed for histological studies and microscopic lung metastases (diameter < 0.1 mm) were counted under a microscope at 125× magnification in fields with 0.32 mm diameter. Liver, kidney, spleen, and adrenals were removed and processed in the same way, looking for macro- and micrometastatic foci.

Supernatant of Dissociated Tumor Tissues

Samples of 1×10^8 cells from MC-C, S-180, 2P-2, and C7HI tumors were minced and homogenized in 10 ml of ice-cold PBS. Subsequently, supernatant of these dissociated and homogenized tumor tissues was obtained after centrifugation at $8000 \times g$ for 10 min, passed through a 0.2-μm filter, and stored at −20°C until use.

DNA Isolation

Genomic DNA samples of MC-C, S-180, C7HI, and 2P-2 tumors from mice displaying both a bad (B) and a good (G) health condition were obtained by standard phenol-chloroform method and ethanol precipitation (21). As a positive control, the Molt-4 cell line heterozygous for codon 12 (GGT-TGT) (erythroblastoid human cell line) was used.

NRAS *Mutation Analysis*

The universal heteroduplex generator (UHG) stock and genomic DNA were amplified separately and then the UHG/sample heteroduplex was obtained by the mix and melt procedure as previously described (22). The UHG is a PCR product that contains an insertion of 3 cytosines between codon 12 and 13 within exon 1 NRAS gene. That PCR product was purified and resuspended in 100 μl of sterile distilled water (UHG stock solution).

The UHG method used enables the identification of codon 12 and 13 mutations. Heteroduplexes were resolved on nondenaturing 20% (2.6% cross-linked) polyacrylamide gel electrophoresis (PAGE) with 2× TBE (90 nM Tris/HCl, pH 8.35, 90 mM boric acid, 1.25 mM EDTA) in the gel matrix and 1× TBE as running buffer, for 5–6 h at 100 V at room temperature using a Mini-Protean II electrophoresis cell ($7.3 \times 10.2 \times 0.1$ cm) (Bio Rad, CA, USA). The single-strand conformation polymorphism (SSCP) analysis was performed after adding formamide dye mixture (95% formamide; 20 mM EDTA; 0.05% xylene cyanol, 0.05% bromo phenol blue) to the PCR products. The mixtures were heated at 94°C for 5 min, and then loaded onto 12% and 15% PAGEs (29:1 acryl/bisacrylamide). Electrophoresis was performed as mentioned above but at 75 V and 4°C. PAGEs were analyzed by silver staining.

RNA Isolation

Total RNA was extracted aseptically from normal and tumor tissues with SV Total RNA Isolation System (Promega, Madison, WI, USA), according to the manufacturer's instructions. Briefly, 50–100 mg of frozen tissue was immersed in 1 ml of SV lysis buffer and homogenized with a Polytron homogenizer. After dissolution in RNase-free distilled water, RNA concentration was spectrophotometrically quantified and quality checked by gel electrophoresis.

RT-PCR

For RT-PCR reactions, one step RT-PCR access (Promega) was used following the manufacturer's instructions. Total RNA (1 g) was incubated with 5× AMV/Tfl reaction buffer, 1 μl of 10 mM dNTP, 2.5 μl of 25 mM $MgSO_4$, 50 pmol of primers, 1 μl of AMV reverse transcriptase (5 U/μl), 1 μl of Tfl DNA polymerase (5 U/ μl), and nuclease-free water to a final volume of 50 μl and one drop of mineral oil for 45 min at 42°C to generate cDNA first strand. Following this, PCR reaction was performed in the same tube without removal from the thermocycle. Preliminary experiments were performed to determine the right cycle number for amplifying cDNA from each gene product during the exponential phase of PCR. Reaction cycle versus product yield curves of tumor RNA were plotted on semilogarithmic graphs. We chose the number of cycles within the linear phase. The number of cycles selected were: 35 cycles for TNF-α and IL-1β and 20 cycles for IL-6.

Determination of TNF-α, IL-1β, and IL-6 in Serum and Tumor Tissues

TNF-α activity was determined in serum and supernatant of dissociated tumor tissues by a cytotoxic assay

using L-929 cells as target, as previously described (23). Titer of TNF-α activity was expressed as the reciprocal of the dilution producing 50% cytotoxicity on L-929 cells and expressed as lytic units (LU) 50 by 0.1 ml. Specificity of the assay was confirmed by the ability of an anti-TNF-α antibody (Sigma, St. Louis, MO, USA) and a TNF-α receptor (see below) to abrogate the cytotoxicity of L-929 cells produced by test samples. The presence of IL-1β and IL-6 in serum and supernatant of dissociated tumor tissues was determined by ELISA (R&D Systems, Minneapolis, MN, USA).

Anti-TNF-α Therapy

Recombinant fusion protein composed of soluble dimeric human p80 tumor necrosis factor-α receptor (TNFR) linked to the Fc region of human IgG (TNFR: Fc, etanercept) was purchased from John Wyeth (Buenos Aires, Argentina). In vivo neutralization of serum TNF-α activity from tumor-bearing mice was attempted by IV inoculation with 100 μg of TNFR/Fc per mouse in 0.1 ml of saline as previously described (24). TNF-α activity present in the serum was evaluated at selected periods after anti-TNF-α therapy.

Antimacrophage Therapy

Clodronate (dichloromethylene bisphosphonate) was provided by Roche Diagnostics (Mannheim, Germany). Liposomal-encapsulated clodronate was prepared using 86 mg of phosphatidylcholine (Lipoid EPC, Lipoid, Ludwigshafen, Germany), 8 mg of cholesterol (Sigma), and clodronate (0.7 mol/L) in a final volume of 4 ml as previously described (25). Empty liposomes were prepared under the same conditions in phosphate-buffered saline. Mice bearing 100–150 mm^3 tumors were anesthetized and then received an intratumoral (IT) and an IV inoculation of 0.1 ml/10 g body weight of this liposomal-encapsulated clodronate suspension. The IV injection of this suspension induced the complete depletion of splenic and hepatic macrophages within 24 h as previously reported (25). Tumor-bearing mice receiving empty liposomes served as controls.

Statistical Analysis

Student's *t*-test, Mann Whitney U-test, and chi-square were used. Values were expressed as mean ± SE). Differences were considered significant when a value was $P = 0.05$ or smaller.

RESULTS

Relationship Between Tumor Mass and Health Condition of Tumor-Bearing Mice

To determine the relationship between tumor mass and the damage to the organism, groups of syngeneic mice were inoculated SC with 1×10^5 cells from the following tumors: MC-C ($n = 24$); S-180 ($n = 13$); 2P-2 ($n = 30$), and C7HI ($n = 28$). Animals were observed daily and the kinetics of tumor growth were registered in all groups. When a mouse exhibited a bad (B) health condition, the mouse was sacrificed and the tumor was excised and weighed and then prepared for histological studies and DNA and RNA analysis. At the same time, if there existed another mouse bearing a tumor of similar volume but displaying a fair (F) or a good (G) health condition, that mouse was also sacrificed and the tumor weighed and prepared as above for histological and molecular studies.

As shown in Figure 1a, sharp differences in tumor mass were found in 12 MC-C tumor-bearing mice exhibiting a B health condition with significant differences between the six lower and the six higher tumor masses (2.8 ± 0.3 g vs. 5.8 ± 0.8 g, $P < 0.01$) detected at 49.7 ± 1.4 days versus 60.5 ± 1.3 days of tumor growth, respectively ($P < 0.001$), with extreme values of 1.9 g and 9 g registered at 45 and 65 days of tumor growth, respectively. Figure 1a also shows that there were B mice bearing a tumor mass (2.1 ± 0.4 g, $n = 3$, at 47 1.1 days of tumor growth) more than three times smaller than that of other mice displaying a G health condition (6.9 ± 1.1 g, $n = 2$ at 64 ± 1 days of tumor growth, $P < 0.02$). As shown in Figure 1b–d, similar results to those for MC-C tumor were observed with S-180, 2P-2, and C7HI tumors.

Results of the above experiments showed that a larger primary tumor mass would not necessarily be associated with a worse health condition. In another experiment, a similar conclusion was reached concerning secondary tumor mass. In effect, C7HI tumor-bearing mice exhibiting a B health condition ($n = 17$) showed a higher, equal, or even lower metastatic load than that observed in mice bearing a similar primary tumor mass and the same length of tumor growth but displaying a F ($n = 27$) or a G health condition ($n = 24$) (Fig. 2). Metastatic load of C7HI tumor-bearing mice was restricted to lung because no macro- or micrometastatic foci were detected in liver, kidney, spleen, and adrenals. Study of the relationship between metastatic load and health condition was limited to C7HI tumor-bearing mice, because MC-C, S-180, and 2P-2 tumor-bearing mice did not display metastatic growth.

Search for NRAS *Mutations in Tumor Cells Derived From B and G Hosts*

To understand the mechanisms by which some mice bearing small tumors died rapidly while others displayed a G health condition bearing similar or even larger tumors, a genomic DNA analysis for *NRAS* mutations was

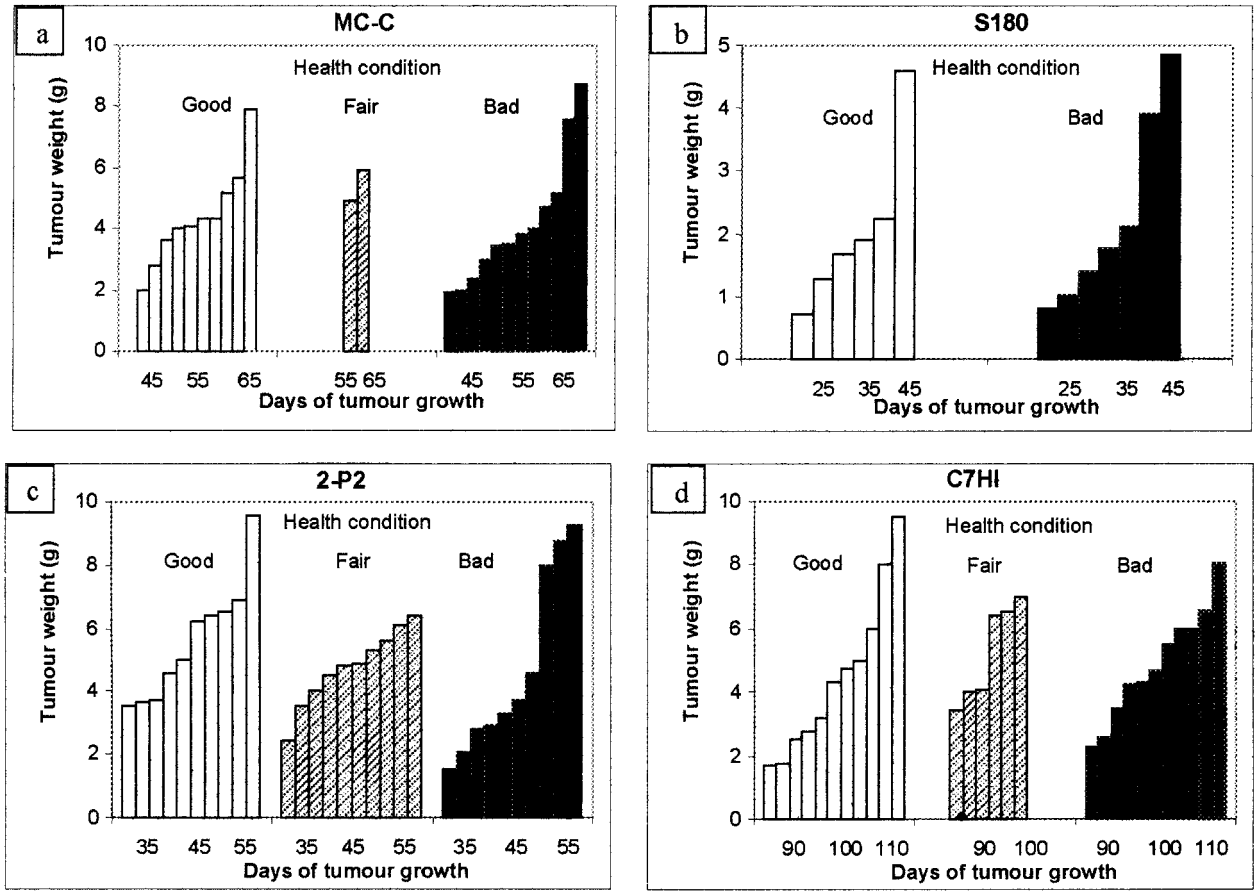

Figure 1. Study of the relationship between tumor mass (ordinate) and health condition of tumor-bearing mice. Tumor growth was initiated with a subcutaneous implant of 1×10^5 cells either of (a) methylcholantrene-induced fibrosarcoma, MC-C; (b) spontaneous sarcoma, S-180; (c) spontaneous lymphoma, 2P-2; or (d) medroxyprogesterone-induced mammary adenocarcinoma, C7HI. Abscissa represents days of tumor growth. Each column represents a single tumor.

performed in cells from tumors of similar size growing either in B or G mice. Rationale for this study was based on the claim that wild-type *NRAS* can suppress or reduce malignant properties of murine tumor cells even in the absence of its oncogenic allele, suggesting that *NRAS* mutations could act as a general enhancer of the transformed phenotype (6). Our results would not support that expectation for the tumors studied herein. In effect, two independent samples of MC-C, S-180, C7HI, and 2P-2 tumors from both B and G hosts showed the same pattern as the normal one for the hot codons 12 and 13 either by the UHG method or the SSCP method. A representative experiment with S-180 and C7HI tumors is shown in Figure 3. Mass of MC-C tumor from B (4.1 $\pm$ 0.2 g) and G mice (4.4 $\pm$ 0.2 g) was not significantly different. The same was also valid for S-180 (1.9 $\pm$ 1 g for B vs. 1.8 $\pm$ 1 g for G mice), 2P-2 (6.3 $\pm$ 1.8 g for B vs. 5.7 $\pm$ 0.9 g for G mice), and C7HI (4.8 $\pm$ 0.4 g for B vs. 4.6 $\pm$ 0.4 g for G mice) tumors.

Although mutations in other proto-oncogenes might underlie the different tumor aggressiveness of our murine tumors, the following in vivo experiments did not favor that possibility. In effect, 1×10^5 MC-C live tumor cells derived from tumors of similar size growing either in B or G hosts were inoculated SC in normal mice. Survival time of mice that received tumor cells from B hosts was 55.3 $\pm$ 1.8 days (n = 12; range 45–65 days), not significantly different from that of mice receiving tumor cells from G hosts: 53.3 $\pm$ 1.9 days (n = 30; range 39–73 days). Kinetics of tumor growth was also similar in both groups. The same results were obtained with S-180, 2P-2, and C7HI tumor cells. This suggested that the deleterious effect observed in B hosts could not be due to a more aggressive subpopulation of tumor cells present in tumors from B but absent in those from G hosts.

Histopathological Studies

Murine Tumors. Three different areas were distinguished within the four tumors studied herein: the live and the necrotic zones, and a third intermediate area that

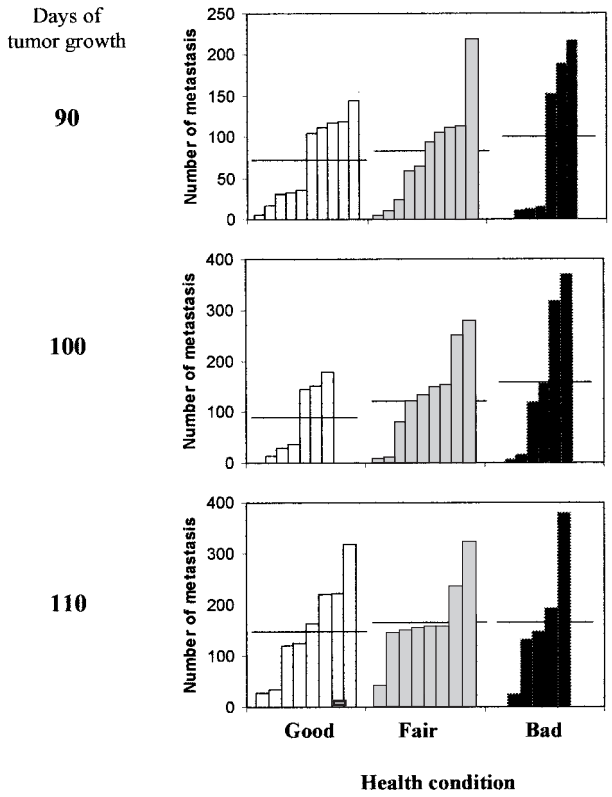

Figure 2. Study of the relationship between number of surface lung metastases (>0.1 mm) and health condition of mice bearing a subcutaneous C7HI tumor at 90, 100, and 110 days of tumor growth. Each column represents a single mouse. Ordinate: number of surface lung metastases. Abscissa: host health condition. Horizontal lines represent the mean of metastatic foci for each group. Differences among groups were not significant. No difference was found for microscopic metastases (<0.1 mm) either (data not shown).

we have designated the transition zone (Fig. 4a). The live zone was characterized by the presence of both actively proliferating tumor cells and a complex network of capillaries. The number of mitotic images was high in MC-C, S-180, and 2P-2 tumor models and relatively scanty in C7HI. In all cases, mitoses were more frequent distant from the boundaries of the necrotic areas than nearby. Live zone appeared either as a ring in the periphery of the tumor (such as in MC-C), or as discrete bundles radially located between the periphery and the core of the tumor mass (such as in S-180, 2P-2, and C7HI). The necrotic zone appeared in the core of the tumor or scattered as irregular bands among areas of live tissue, sometimes displaying hemorrhagic and liquefaction necrotic foci and localized areas of dystrophic calcification. The transition zone appeared between the live and necrotic zones; scattered live tumor cells coexisted with degenerating, apoptotic, and necrotic tumor cells along with cellular and nuclear debris resulting from different stages of cellular disintegration. Depending on each type of tumor, the transition zone showed a variable width and a different density of stroma (cells and extracellular matrix).

A careful histopathological analysis of the three tumor zones in mice exhibiting different health conditions was carried out. No cytological differences could be found among live tumor cells derived from B, F, and G hosts. Similarly, although tumors from B hosts usually showed a significantly higher proportion of necrosis than tumors of a similar mass growing in G hosts, this difference could not be considered as a reliable index of a worse health condition. For example, as shown in Table 1, the percentage of necrosis of large MC-C tumors in G hosts was actually higher than that observed in small MC-C tumors from B hosts ($P < 0.05$). In our hands, the main morphological difference between tumors from B and G hosts, independently of tumor size, was the sharply higher number of small, sinuous, and dilated capillaries inside the transition tumor zone from B compared with those from G mice; some of these vessels were also seen penetrating into the necrotic zone (Table 1, Fig. 4a vs. b and c). Tumors from F mice gave an intermediate image. It is worth noting that the number of capillaries in the live zone was not pertinent to predict health condition (Table 1). For example, MC-C tumors 2–3 g in weight from B hosts displayed a lower number of capillaries/field in the live zone than in similar-sized MC-C tumors from G hosts (17.2 vs. 27.2, respectively) while, on the other hand, the number of capillaries/field in the transition area was dramatically increased (37.5 in B vs. 3.4 in G hosts).

Considering only tumors from B hosts, a significant difference could be detected between tumors displaying a more or a lesser aggressive behavior. In effect, as shown in Table 1, in small S-180 and MC-C tumors that induced a rapid deleterious effect on the organism, swelling capillaries inside transition areas were filled with inflammatory cells (macrophages, mononuclear, and polymorphonuclear), eventually migrating outside the capillaries. On the other hand, in large MC-C and in the slow growing C7HI tumors, which induced a late deleterious effect, no inflammatory cells were seen inside capillaries or infiltrating tumor tissues ($P < 0.01$, compared with the inflammatory infiltration grade observed in small MC-C and S-180 tumors, which induced a rapid deleterious effect on the organism), nor was an inflammatory response detected in lung C7HI metastatic foci. The 2-P2 tumor could not be evaluated in this way because its lymphoid nature made it difficult to discriminate between tumor and inflammatory infiltrating cells.

Human Tumors. Out of 80 samples analyzed, 56 displayed the three zones of live, necrotic, and transition areas described in our murine tumors; three representa-

tive examples are shown in Figure 5. The remaining 24 tumors exhibited only the live zone. The percentage of carcinomas exhibiting the three zones (63%, 41 out of 65) was significantly lower than that observed in sarcomas, lymphomas, and tumors of the nervous system (100%, 15 out of 15, $P < 0.05$). In the latter, transition zones were in all cases characterized by the presence of a high number of small vessels and inflammatory cells with intra- and extravascular localization. On the other hand, in carcinomas, transition zones displayed vascularization in only 26 out of 41 cases and the number of vessels was, in general, lower than that observed in the other tumors.

Transition and Necrotic Zones as a Source of Cachectic Factors

An IV inoculation in normal mice of supernatant of dissociated transition and necrotic tissues from MC-C, S-180, 2P-2, and C7HI tumors induced a syndrome similar to the cachectic situation in a dose-dependent man-

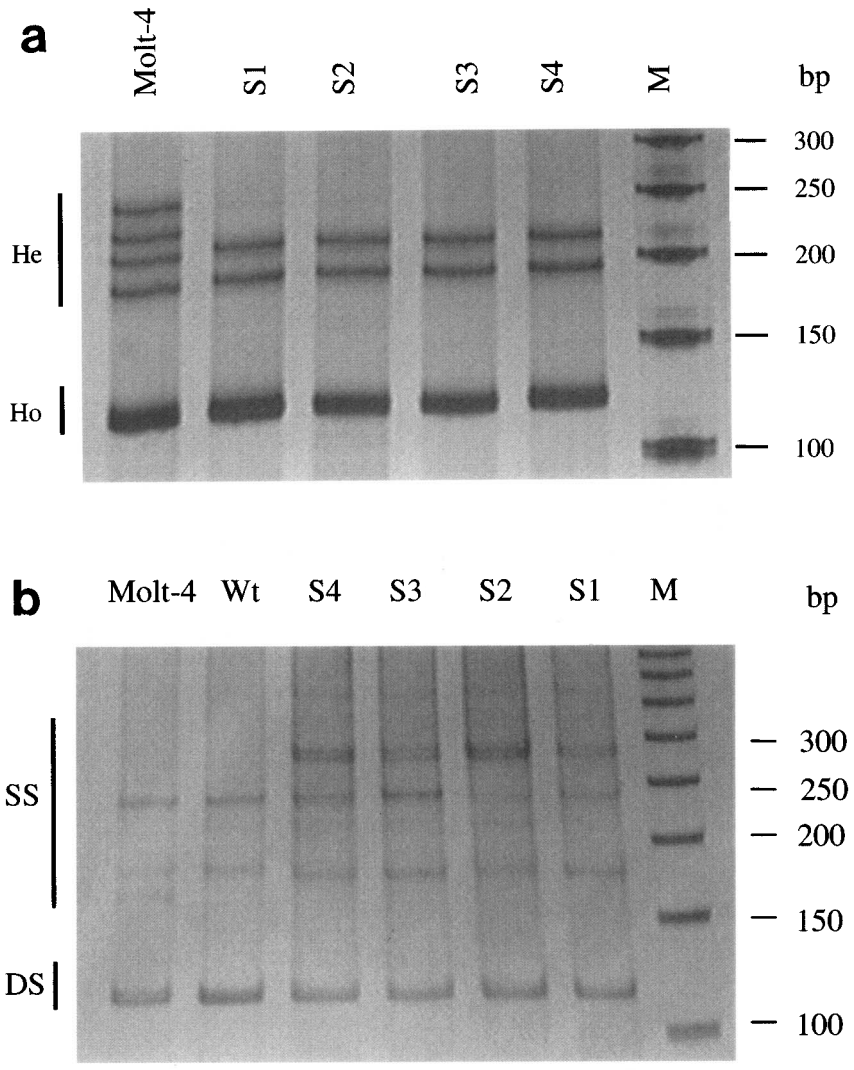

Figure 3. Search for *NRAS* mutations in tumors from BALB/c mice. S1: S-180 tumor from mice exhibiting good health condition. S2: S-180 tumor of similar size as S1, from mice exhibiting bad health condition. S3: C7HI tumor from mice exhibiting bad health condition. S4: lung from a normal mouse. Molt 4: erythroblastoid human cell line heterozygous for codon 12. Wt: blood sample from a healthy human donor. M: 50 bp molecular size marker. (a) Silver-stained patterns obtained from mouse samples (S1–S4) analyzed by heteroduplex analysis using the UHG under nondenaturing mini-gel electrophoresis (7 cm long). He: heteroduplex; Ho: homoduplex. (b) Silver-stained patterns of mouse samples (S1–S4) obtained by SSCP analysis (15%) (7 cm long). SS: single-strand DNA; DS: double-strand DNA.

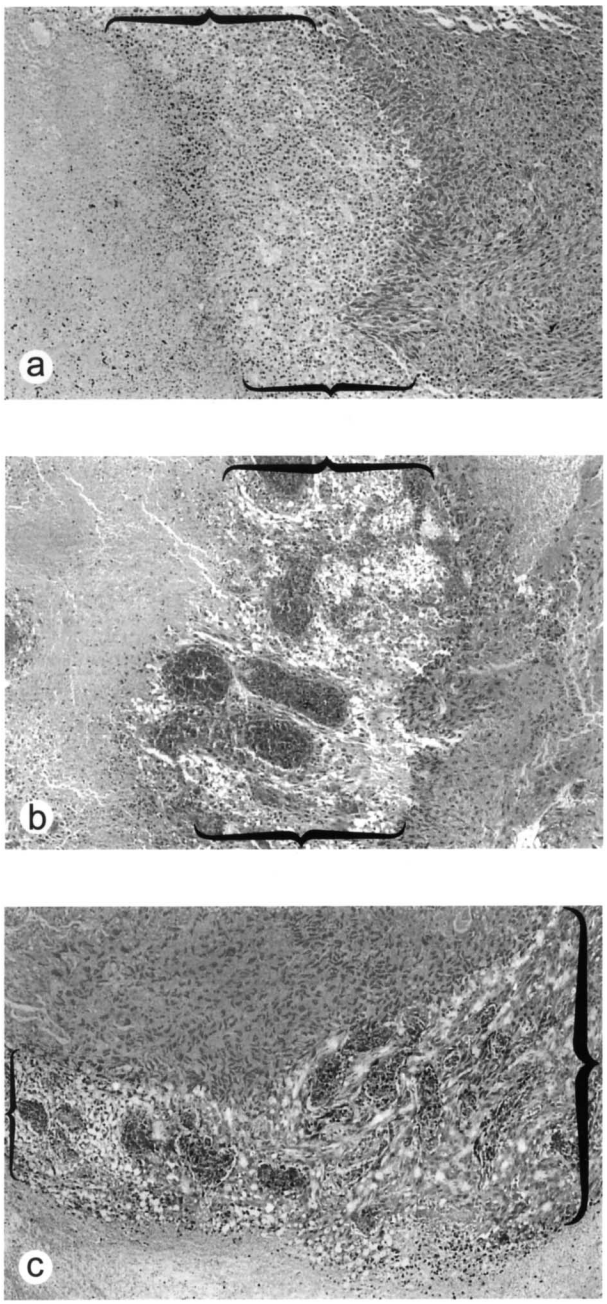

Figure 4. Murine tumors. (a) MC-C fibrosarcoma from a mouse displaying a good health condition showing the transition (between brackets), the live (right), and the necrotic (left) zones. In the poorly vascularized transition zone, see scattered live, apoptotic (with pycnotic nuclei), and degenerative tumor cells (mainly near the edge of the necrotic zone). H&E ×10. (b) MC-C fibrosarcoma from a mouse displaying a bad health condition. Between the live (right) and necrotic (left) zones, the transition zone (between brackets) shows dilated and congestive vascular structures and hemorrhagic foci. Inflammatory cells are observed both inside and outside of the vascular structures. H&E ×10. (c) S-180 sarcoma from a mouse displaying a bad health condition. Between the live (upper) and necrotic (lower) zones, the transition zone (between brackets) shows irregular, dilated, and congestive vascular structures with a dense inflammatory cell infiltration. H&E ×10.

ner. On the other hand, no harmful effect was observed with supernatant of dissociated live tumor tissues (data not shown). These results suggest that cachectic factors are produced or released by dying tumor cells placed in the transition and necrotic zones. The fact that treatment of tumor-bearing mice with liposomal encapsulated clodronate–a macrophage-depleting agent–diminished the cachectic activity of supernatant of transition and necrotic tumor tissues in two models (MC-C and 2P-2) raised the possibility that tumor-infiltrating macrophages could be an additional source of cachectic factors. To investigate the nature of these factors, RT-PCR analysis for mRNAs of TNF-α, IL-1β, and IL-6 was carried out in the tumor tissue and in the liver of tumor-bearing mice displaying a bad health condition. For MC-C and S-180 tumors, TNF-α mRNA was detected in the transition and necrotic areas but not in the live tumor area or in the liver of tumor-bearing mice. For 2P-2 and C7HI tumors, low TNF-α mRNA levels were observed in all tumor zones. IL-1β mRNA was expressed in all tumor zones in S-180 tumor and in the liver of S-180 tumor-bearing mice; on the other hand, IL-1β mRNA was expressed only in the transition and necrotic zones of C7HI tumor. IL-6 mRNA was undetectable in all tumors. A representative experiment is shown in Figure 6.

The presence of TNF-α, IL-1β, and IL-6 in serum and tumor tissues was evaluated in tumor-bearing mice exhibiting a bad or a good health condition. As shown in Table 2, a direct proportionality between circulating TNF-α and worse health condition was observed in mice bearing MC-C (group I vs. II) and S-180 (group III vs. IV) tumors. On the other hand, no TNF-α over control values was detected in the serum of C7HI and 2P-2 tumor-bearing mice displaying a bad health condition, suggesting that in these models worsening of health state would be unrelated to TNF-α. Moreover, an amazing improvement of health and prolonged survival were observed in 15 MC-C and 12 S-180 tumor-bearing mice after an anti-TNF-α therapy by receiving three weekly IV injections of TNF-α receptor linked to the Fc region of human IgG (TNFR/Fc). Survival time of MC-C tumor-bearing mice was 52.3 ± 2.0 days for TNFR/Fc recipients versus 32.2 ± 2.1 days for controls ($P < 0.001$). Survival time of S-180 tumor-bearing mice was 57.4 ± 3.0 days for TNFR/Fc recipients versus 27.2 ± 2.2 for controls ($P < 0.001$). It is worth noting that in both MC-C and S-180 models recovery of health after TNFR/Fc treatment was paralleled with a sharp drop in TNF-α concentration in serum and it occurred despite the fact that tumor size was progressively increased. In contrast, the health of four C7HI and four 2P-2 tumor-bearing mice was not improved by treatment with TNFR/Fc (data not shown). In the same way, intratumor (IT) TNF-α, mostly in the transition and necrotic zones, was found

Table 1. Correlation Between the Number of Capillaries and the Grade of Inflammatory Infiltration Observed in the Tumor Transition Zone and the Health Condition of Tumor-Bearing Mice

Tumor	Mass (g)	Health Condition	% Necrosis	No. of Capillaries/Field: Live Zone	No. of Capillaries/Field: Transition Zone	Poly- and Mononuclear Infiltration (Grade)	*N*
MC-C	2–3	B	44.3	17.2 ± 2.2	37.5 ± 2.7	3	6
		G	25.5	27.2 ± 2.6*	3.4 ± 1.3†	1	9
	4–5	B	50.5	13.0 ± 2.9	27.6 ± 2.4	2	5
		F	36.3	5.3 ± 2.4	8.3 ± 2.4‡	3	3
		G	34.0	7.0 ± 2.1	5.2 ± 1.9†	0	5
	6–9	B	66.6	5.5	15.5	0	2
		G	56.2	1.5	0.5§	0	2
S-180	1–2	B	64.0	48.8 ± 3.7	50.8 ± 4.7	2	4
		G	43.0	5.2 ± 1.2†	6.2 ± 1.1†	0	5
	2–4	B	51.0	6.7 ± 1.2	36.3 ± 4.5	1	4
		G	49.0	5.5	2.5¶	0	2
C7HI	4–6	B	58.1	6.9 ± 0.9	12.0 ± 2.7	0	6
		F	50.5	5.3 ± 1.3	1.8 ± 0.6#	0	4
		G	37.5	2.5 ± 1.3	0.3 ± 0.3¶	0	4
2-P2	3–5	B	38.6	22.6 ± 3.4	36.3 ± 5.4	—	3
		F	33.5	8.3 ± 1.2¶	11.3 ± 1.7‡	—	5
		G	34.3	4.0 ± 0.6†	1.6 ± 0.2†	—	5

Values for the live and transition zones represent the mean ± SE of *n* tumors; values without the SE are averages of only two values and SEs were not included. Data from each tumor were obtained by averaging the number of capillaries of 10 fields of 0.4-mm diameter. For simplicity, for percent of necrosis and poly- and mononuclear infiltration grade, only mean values are shown; SE was always <15% of mean value. Health condition was rated as: G (good)—similar state to that of control mice without tumor; F (fair)—incipient signals of health impairment; B (bad)—bristling hair, weight loss up to 20% of the body weight at the start of the experiment, reduced mobility, and dyspnea without cyanosis. Grade of poly- and mononuclear infiltration was determined according to Mancini et al. (20).
*Significantly higher than in B ($P < 0.01$).
†Significantly lower than in B ($P < 0.001$).
‡Significantly lower than in B ($P < 0.002$).
§Significantly lower than in B ($P < 0.02$).
¶Significantly lower than in B ($P < 0.01$).
#Significantly lower than in B ($P < 0.05$).

in MC-C and S-180 tumors, but not in C7HI and 2-P2 tumors. However, different from what was observed with circulating TNF-α, no correlation between TNF-α, concentration in MC-C and S-180 tumor tissues, and worse health condition was detected (Table 2). A direct proportionality between circulating IL-1β titer and worse health condition was observed in C7HI tumor-bearing mice (120.4 ± 2.0 pg/ml in B mice, $n = 4$ vs. 26.5 ± 2.5 pg/ml in G mice, $n = 4$, $P < 0.001$) but not in MC-C, S-180, and 2P-2 tumor-bearing mice. In addition, similar to what was observed with TNF-α, no correlation between IL-1β present in C7HI tumor tissues (mostly in the transition and necrotic zones) and worse health condition was detected (data not shown). For IL-6, no concentration of this cytokine over control values was detected in both serum and tumor tissues from MC-C, S-180, 2P-2, and C7HI tumor-bearing mice. Serum from 2P-2 tumor-bearing mice displaying a bad, but not a good, health condition, exhibited a cachectizing-like effect when inoculated IV into normal mice. This effect could be attributed to a not yet characterized dialyzable (MW < 12500 Da), heat-resistant (56°C 0.5 h), and nonpeptidic factor that was also observed in the transition and necrotic 2P-2 tumor tissues whatever the health condition of 2P-2 tumor-bearing mice (data not shown). Taken together, the results suggested that different cachectic factors could be produced in tumor transition and necrotic tissues from tumor-bearing hosts exhibiting both a bad and a good health condition; however, only in the former (bearing tumors with highly vascularized

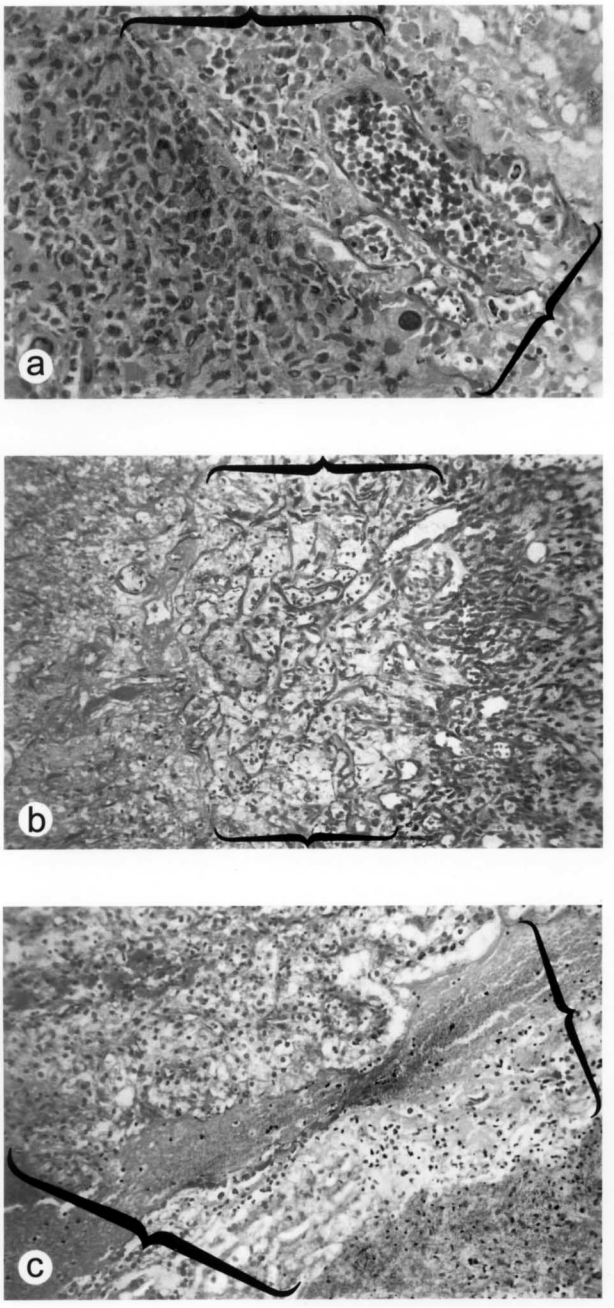

Figure 5. Human tumors. (a) Malignant astrocytoma with presence of a well-defined transition zone (between brackets) between the live (left) and necrotic (right) zones. The transition zone shows a mixture of preserved, apoptotic, and degenerative tumor cells with numerous, irregular microvessels and a giant capillary containing scanty intraluminal tumor and inflammatory cells. H&E ×25. (b) Malignant schwannoma. Between the live (right) and necrotic (left) zones, the transition zone (between brackets) shows a higher number of irregular capillaries; inflammatory cells are seen inside these vessels and infiltrating tumor tissue. H&E ×25. (c) Clear cell renal carcinoma. Between the live (upper left) and necrotic (lower right) zones, the transition zone (between brackets) shows an extensive hemorrhagic area with a giant capillary and scattered preserved and degenerating cancer and inflammatory cells. H&E ×25.

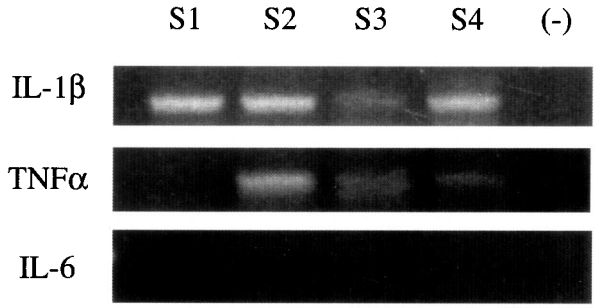

Figure 6. Levels of IL-1β, TNF-α, and IL-6 mRNA were analyzed by RT-PCR in the live zone of S-180 tumor (S1), transition and necrotic zones of S-180 (S2) and C7HI (S3) tumors and in the liver of an S-180 tumor-bearing mouse (S4). Negativel control (-) was liver of normal mice. RNA concentrations were internally controlled using the housekeeping gene β-actin. Intensity of the bands of β-actin was identical in all cases (data not shown).

Table 2. Concentration of TNF-α in Serum and Tumor Tissues of Tumor-Bearing Mice Displaying Different Health Conditions

				Tumor Tissues	
Tumors	Tumor Weight (g)	Host Health	Serum	Necrotic and Transition	Live
I. MC-C	4	bad	4.33*	6.42	1
II. MC-C	4	good	1.26*	10.69	1
III. S-180	3	bad	6.49†	16.79‡	4.47
IV. S-180	3	good	1.43†	5.73‡	1
V. C7HI	5	bad	1	1.44	1
VI. 2P-2	4	bad	1	1	1

Values for serum and tumor tissues are the ratio of TNF-α titer of serum and supernatant of dissociated tumor tissues from tumor-bearing mice to TNF-α titer of normal serum and tissues. Titer of TNF-α was calculated as the reciprocal of serum or tissue sample dilution producing 50% cytotoxicity on L-929 cells and expressed as lytic units (LU) 50 by 0.1 ml. For simplicity only mean values are shown; standard error (SE) was always 15% of mean value. The determination of TNF-α in serum of MC-C tumor-bearing mice was the mean of 5 experiments; of S-180 tumor-bearing mice the mean of 3 experiments; and of C7HI and 2P-2 tumor-bearing mice the mean of 2 experiments. Control normal serum displayed a TNF-α titer of 10.80 ± 2.33 LU_{50}/0.1 ml (mean ± SE of 5 experiments), corresponding to 10.26 pg/ml of TNF-α. The determination of TNF-α in tumor tissues of MC-C and S-180 tumor-bearing mice was mean of 3 experiments; and of C7HI and 2P-2 tumor-bearing mice the mean of 2 experiments. Control normal spleen and kidney tissues displayed a TNF-α titer of 12.98 ± 3.41 LU_{50}/0.1ml of supernatant of dissociated normal tissues (100 mg/ml) in saline (mean ± SE of 3 experiments), corresponding to 14.79 pg/ml of TNF-α.
*$P < 0.02$.
†$P < 0.01$.
‡$P < 0.05$.

transition zone) could these factors reach the general circulation while in the latter (bearing tumors with poorly vascularized transition zone) passage of these factors to the general circulation seemed to be diminished or precluded.

DISCUSSION

The biological behavior of a neoplastic disease is not always fully understood on the basis of classical criteria such as tumor burden and extent of spread (4). This raises the possibility that other criteria in addition to the classical ones might help us to predict more accurately the outcome of malignant tumors as well as to serve as a guide for choosing the best treatment.

In this article, studying the growth of four different murine tumors, we observed that a larger primary and secondary tumor load with a longer length of growth would not necessarily be a reliable index of a worse prognosis and, reciprocally, that apparently identical tumors, with similar mass and the same length of growth, could have sharply different effects on the host's health condition. In addition, the relatively benign behavior of one of the tumors studied (the mammary adenocarcinoma called C7HI) seems to contradict the claim that a highly malignant behavior is associated with rapid dissemination and metastases. In this case, although development of lung metastases begins early, deleterious effects on the organism usually occur very late during tumor growth. Of course, this is not to say that metastases are not an important cause of death, but it suggests that other deleterious factors could also be involved.

The term "progression" has been coined to describe a change from a relatively harmless to a more harmful tumor behavior associated with the emergence of a more malignant subpopulation of tumor cells (26). The enhanced aggressiveness of our tumors, however, does not fall easily within that interpretation. In effect, no differences in cytological images or in *NRAS* mutations (claimed to be related to a more aggressive tumor behavior in some murine systems) were observed among live tumor cells from similar size tumors derived from mice exhibiting a bad, fair, or good health condition. In addition, no differences in both tumor kinetics and survival time were detected among naive mice receiving an implant of live tumor cells whatever the health condition of the donor mouse. Another possibility could be related to a differential vascular supply of the live tumor tissue. In effect, it is known that growth of solid tumors beyond a small volume must be preceded by an expansive angiogenic development (27–29). On this basis, considering two otherwise identical tumors, the conventional theory assumes that the one that displayed a higher number of capillaries irrigating the live tissue would attain a larger

mass and in consequence would kill the host earlier (30,31). However, by comparing similar size tumors with the same length of growth, our observations showed that a higher number of vessels into the live tumor tissue was not necessarily correlated with a worse prognosis. A third possibility was associated with the presence of tumor necrotic areas, which have been known for many years to correlate with a bad prognosis in some human tumors (32–35). However, in our murine models, necrosis itself was not always a clear-cut index of a more aggressive tumor behavior. In effect, although tumors from hosts displaying a bad health condition usually showed a higher percentage of necrosis than similar size tumors growing into healthy hosts, small and highly aggressive tumors inducing rapid death of their hosts displayed, in fact, a lower percentage and a smaller total amount of necrosis than larger ones exhibiting a relatively benign behavior.

In our models, the main tumor feature consistently associated with a bad host's health condition, independent of tumor size, was the presence of a high number of small dilated vessels inside the tumor area that we have designated the transition zone. Some of these vessels were also seen penetrating into the necrotic tissue. In addition, when a bad health condition was attained associated with a small tumor mass, that is when tumor behavior was highly aggressive, a high number of mononuclear and polymorphonuclear inflammatory cells was seen inside those vessels and infiltrating tumor tissues. Although live and necrotic areas have been largely studied by former authors, the transition zone, to our knowledge, has not been previously recognized as a distinct structure inside the tumor mass. This zone, placed between live and necrotic areas, where scattered live, dying, apoptotic, and necrotic tumor cells coexist, is probably the most complex intratumor microenvironment, especially in highly aggressive tumors where a dense network of small vessels and an acute inflammatory reaction resemble the morphological traits observed in a wound-healing process in response to tissue injury (7,36,37). On the other hand, in tumors derived from hosts exhibiting a good health condition, practically no small vessels penetrating into transition and necrotic areas or inflammatory reactions were found; intermediate traits to those described above were seen in tumors from mice displaying a fair health state. A retrospective study on human tumor slides revealed that histological images representing the live, transition, and necrotic zones were also observed in biopsies of 100% of sarcomas and tumors of nervous system, 63% of carcinomas, and in the only non-Hodgkin's lymphoma analyzed. Moreover, a high grade of vascularization and a strong inflammatory reaction inside the transition zone were observed in some tumor samples, raising the possibility that in human tumors, these histological images might have a similar prognostic value as in our murine tumors.

When normal mice received an IV inoculum of a supernatant of dissociated transition and necrotic tumor tissues, cachectic symptoms developed in a dose-dependent manner; in contrast, a supernatant of live tumor cells was harmless. In the four tumor models studied herein, this cachectizing effect associated with the transition and necrotic zones was observed independently of the presence of tumor infiltrating inflammatory cells, suggesting that it was dependent mainly on factors produced by dying tumor cells present in those zones. The fact that treatment of tumor-bearing mice with liposomal-encapsulated clodronate–a macrophage-depleting agent–diminished the cachectic activity of the supernatant of transition and necrotic tissues in two out of four models raised the possibility that tumor-infiltrating macrophages could be an additional source of cachectic factors. One of these factors could be TNF-α. In effect, a high concentration of TNF-α was detected in the serum of MC-C fibrosarcoma and S-180 sarcoma-bearing mice displaying a bad health condition, while similar size tumors, associated with good health, did not show values of TNF-α above control. Reciprocally, a dramatic lowering of circulating TNF-α, reversion of cachectic symptoms, and a largely prolonged survival time were observed in MC-C and S-180 tumor-bearing mice after in vivo treatment with an anti-TNF-α therapy by using a dimeric tumor necrosis factor receptor. In contrast, TNF-α did not seem to play a role in the development of cachectic symptoms associated with the mammary adenocarcinoma C7HI and the T-lymphoma 2P-2, suggesting that other molecules could be involved. Il-1β might be implicated in the deleterious effect induced by C7HI tumor because in these mice a direct correlation between circulating IL-1β levels and worse health condition was detected. IL-6 did not seem to play a significant cachectizing role in mice bearing any of the four tumors studied. On the other hand, a heat-resistant, nonpeptidic, and small serum factor could play a main role in the development of cachectic symptoms induced by 2P-2 tumor; according to its physical and chemical properties it was apparently different from any previously postulated cachectic molecules (5). Although in the four models that we studied there was a direct correlation between circulating cachectic factors and a worse health state, concentration of these factors in tumor tissues was similar in tumor-bearing mice exhibiting both a bad and a good health condition, suggesting that only in the former (mice bearing tumors with highly vascularized transition zone) but not in the latter (mice bearing tumors with poorly vascularized transition zone) could these factors reach the general circulation.

All of these considerations may offer a putative ex-

planation why some mice show a short survival time bearing small tumors, while others exhibit a good health state bearing tumors with similar or even larger size. In effect, a small tumor displaying a high number of vessels inside the transition zone (some of them penetrating into the necrotic tissues) could be harmful to its host by allowing its tumor-derived cachectic molecules to reach the capillary drainage and then the general circulation, leading to unbalanced homeostasis, systemic damage, and ultimately death. In contrast, a large tumor could behave as a relatively benign one if its transition (and necrotic) tissues exhibited little or no vascularization and in consequence its cachectic factors were "trapped." In this way, the different aggressiveness of two otherwise identical tumors might be inversely correlated to the time elapsed between the onset of tumor growth and the vascularization of its transition and necrotic tissues. In turn, this period of time seemed to be related to the origin of necrosis. In effect, if necrosis was a consequence of a lack of vascular supply, as it is usually admitted, vascularization of transition and necrotic areas should be a secondary and late event presumably dependent on proangiogenic factors associated with tissue damage and hypoxia (38–41). In this case, death of tumor-bearing host would occur late during tumor development and would be associated with a large tumor mass (relatively benign behavior). On the other hand, the existence of transition and necrotic areas scattered among live tissues in highly vascularized small tumors suggested that necrosis might also occur in the face of a normal vascular supply, putatively induced by products of a precocious inflammatory response to the tumor (39,42,43). In this case, vascularization of transition and necrotic zones and death of tumor-bearing host would be attained early during tumor development and associated with a small tumor mass (highly malignant behavior).

Antiangiogenic and anti-inflammatory schedules (29, 31) might help to prevent the vascularization of the transition and necrotic tumor areas, diminishing the releasing of potentially cachectic factors into the general circulation. In addition, our experiments have shown that appropriate anticachectic treatments can ameliorate or even reverse the cachectic symptoms associated with those factors, suggesting that the deleterious effect of a tumor on the organism might be potentially reversible, even in the case of a tumor-bearing host expected shortly to become moribund.

In conclusion, in this article we have identified in four murine tumors a histologically recognizable tumor structure (i.e., the transition zone) in which both a high number of vessels and a strong inflammatory reaction could be considered a histological hallmark of a highly aggressive tumor behavior. If our observations can be extended to other experimental and human tumors, the detection of that histological image in routine histopathological studies might be an additional tool to understand and predict the outcome of malignant neoplasms.

ACKNOWLEDGMENTS: The authors are grateful to Dr. Christiane D. Pasqualini for critical discussion of the manuscript, to Drs. Coloma Parisi, Irene Larripa, and Fernando Minucci for helpful suggestions, and to Messrs. E. R. Croccito, J. J. Portaluppi, E. da Vinci, A. Morales, and R. Fraiman for expert technical assistance. This work was supported by grants from CONICET (Consejo Nacional de Investigaciones Científicas y Técnicas) and ANPCyT (Agencia Nacional de Promoción Científica y Tecnológica).

REFERENCES

1. Ohori, M.; Wheeler, T. M.; Scardino, P. T. The New American Joint Committee on Cancer and International Union Against Cancer TNM classification of prostate cancer. Clinicopathologic correlations. Cancer 74:104–114; 1994.
2. Sobin, L. H.; Wittekind, C. H. TNM classification of malignant tumors. New York: Wiley-Liss; 1997.
3. Katai, H.; Yoshimura, K.; Maruyama, K.; Sasako, M.; Sano, T. Evaluation of the new International Union Against Cancer and American Joint Committee on Cancer TNM staging of gastric carcinoma. Cancer 88:1796–1800; 2000.
4. Longo, D. L. Oncology and hematology, neoplastic diseases. In: Fauci, A. S., ed. Harrison, principles of internal medicine. New York: McGraw-Hill Inc.; 1998:561–568.
5. Tisdale, M. J. Biology of cachexia. J. Natl. Cancer Inst. 89:1763–1773; 1997.
6. Díaz, R.; Ahn, D.; Lopez-Barcons, L.; Malumbres, M.; Perez de Castro, I.; Lue, J.; Ferrer-Miralles, N.; Mangues, R.; Tsong, J.; García, R.; Pérez-Soler, R.; Pellicer, A. The N-ras proto-oncogene can suppress the malignant phenotype in the presence or absence of its oncogene. Cancer Res. 62:4514–4518; 2002.
7. Coussens, L. M.; Werb, Z. Inflammation and cancer. Nature 420:860–867; 2002.
8. Brigati, C.; Noonan, D. M.; Albini, A.; Benelli, R. Tumors and inflammatory infiltrates: Friends or foes? Clin. Exp. Metastasis 19:247–258; 2002.
9. Kolb, E. Current knowledge of characteristics and effects of alpha and beta necrosis factors (cachectins). Z. Gesamte Inn. Med. 46:139–144; 1991.
10. Strassmann, G.; Masui, Y.; Chizzonite, R.; Fong, M. Mechanisms of experimental cancer cachexia. Local involvement of IL-1 in colon-26 tumor. J. Immunol. 150: 2341–2345; 1993.
11. Billingsley, K. G.; Fraker, D. L.; Strassmann, G.; Loeser, C.; Fliot, H. M.; Alexander, H. R. Macrophage-derived tumor necrosis factor and tumor-derived of leukemia inhibitory factor and interleukin-6: Possible cellular mechanisms of cancer cachexia. Ann. Surg. Oncol. 3:29–35; 1996.
12. Harris, N. L. A revised European–American classification of lymphoid neoplasms: A proposal from the International Lymphoma Study Group. Blood 84:1361–1392; 1994.
13. Kordon, E.; Lanari, C.; Molinolo, A. A.; Elizalde, P. V.; Charreau, E. H.; Pasqualini, C. D. Estrogen inhibition of MPA-induced mouse mammary tumor transplants. Int. J. Cancer 49:900–905; 1991.
14. Franco, M.; Bustuoabad, O. D.; di Gianni, P. D.; Gold-

man, A.; Pasqualini, C. D.; Ruggiero, R. A. A serum-mediated mechanism for concomitant resistance shared by immunogenic and non-immunogenic murine tumours. Br. J. Cancer 74:178–186; 1996.
15. Attia, M. A.; Weiss, D. W. Immunology of spontaneous mammary carcinomas in mice. V. Acquired tumor resistance and enhancement in strain A mice infected with mammary tumor virus. Cancer Res. 26:1787–1800; 1966.
16. Tisdale, M. J. Cancer cachexia. Br. J. Cancer 63:337–342; 1991.
17. Tanaka, Y.; Eda, H.; Tanaka, T.; Udagawa, T.; Ishikawa, T.; Horii, I.; Ishitsuka, H.; Kataoka, T.; Taguchi, T. Experimental cancer cachexia induced by transplantable colon 26 adenocarcinoma in mice. Cancer Res. 50:2290–2295; 1990.
18. Kelly, W. R. Diagnóstico Clínico Veterinario (translation of Veterinary Clinical Diagnosis, 1972). México: Compaía Editorial Continental; 1976:13–14.
19. Cruz-Orive, L.; Weibel, E. R. Recent stereological methods for cell biology: A brief survey. Am. J. Physiol. 258: L148–L156; 1990.
20. Mancini, A.; Rabitti, C.; Conte, G.; Gullota, G.; De Marinis, L. Lymphocytic infiltration in thyroid neoplasms. Preliminary prognostic assessments. Minerva Chir. 48:1283–1288; 1993.
21. Sambroock, J.; Fristch, E. F.; Maniatis, T. Purification of nuclear acids. In: Nolan, C., ed. Molecular cloning: A laboratory manual (3rd ed., E3 Book 3). New York: Cold Spring Harbor University Press; 1989.
22. Belli, C.; De Brasi, C.; Larripa, I. Rapid detection of exon 1 NRAS gene mutations using universal heteroduplex generator technology. Hum. Mutat. 21:132–137; 2003.
23. Wang, A. M.; Creasey, A. A.; Ladner, M. B.; Lin, L. S.; Strickler, J.; Van Arsdell, J. N.; Yamamoto, R.; Mark, D. F. Molecular cloning of the complementary DNA for human tumor necrosis factor. Science 228:149–154; 1985.
24. Mohler, K. M.; Torrance, D. S.; Smith, C. A.; Goodwin, R. G.; Stremler, K. E.; Fung, V. P.; Madani, H.; Widmer, M. B. Soluble tumor necrosis factor (TNF) receptors are effective therapeutic agents in lethal endotoxemia and function simultaneously as both TNF carriers and TNF antagonists. J. Immunol. 151:1548–1561; 1993.
25. Van Rooijen, N.; Sanders, A. Liposome mediated depletion of macrophages: Mechanism of action, preparation of liposomes and applications. J. Immunol. Methods 174:83–93; 1994.
26. Nowell, P. C. The clonal evolution of tumor cell populations. Science 194:23–28; 1976.
27. Folkman, J. Tumor angiogenesis: Therapeutic implications. N. Engl. J. Med. 285:1182–1186; 1971.
28. Rak, J.; Filmus, J.; Kerbel, R. S. Reciprocal paracrine interaction between tumor cells and endothelial cells: The "angiogenesis progression" hypothesis. Eur. J. Cancer 32A:2438–2450; 1996.
29. Carmeliet, P.; Jain, R. K. Angiogenesis in cancer and other diseases. Nature 407:249–257; 2000.
30. Pluda, J. M. Tumor-associated angiogenesis: Mechanisms, clinical implications and therapeutic strategies. Semin. Oncol. 24:203–218; 1997.
31. O'Byrne, K. J.; Dalgleish, A. G.; Browning, M. J.; Steward, W. P.; Harris, A. L. The relationship between angiogenesis and the immune response in carcinogenesis and the progression of malignant disease. Eur. J. Cancer 36: 151–169; 2000.
32. Coley, W. B. The treatment of malignant tumors by repeated inoculations of erysipelas. With a report of ten original cases. Am. J. Med. Sci. 105:447–451; 1893.
33. Sirica, A. E. Chronology of significant events in the study of neoplasia. In: Sirica, A. E., ed. The pathobiology of neoplasia. New York: Plenum Press; 1989:1–24.
34. Mandard, A. M.; Petiot, J. F.; Marnay, J.; Mandard, J. C.; Chasle, J.; de Ranieri, E.; Dupin, P.; Herlin, P.; de Ranieri, J.; Tanguy, A.; Boulier, N.; Abbatucci, J. S. Prognostic factors in soft tissue sarcomas. A multivariate analysis of 109 cases. Cancer 63:1437–1451; 1989.
35. Dang, L. H.; Bettegowda, Ch.; Huso, D. L.; Kenneth, W.; Kinzler, K. W.; Vogelstein, B. Combination bacteriolytic therapy for the treatment of experimental tumors. Proc. Natl. Acad. Sci. USA 98:15155–15160; 2000.
36. Dvorak, H. F. Tumors: Wounds that do not heal. N. Engl. J. Med. 315:1650–1659; 1986.
37. Lee, A. H. S.; Happerfield, L. C.; Bobrow, L. G.; Millis, R. R. Angiogenesis and inflammation in invasive carcinoma of the breast. J. Clin. Pathol. 50:669–673; 1997.
38. Forsythe, J. A.; Jiang, B. H.; Iyer, N. V.; Agani, F.; Leung, S. W.; Koos, R. D.; Semenza, G. L. Activation of vascular endothelial growth-factor gene-transcription by hypoxia-inducible factor-1. Mol. Cell. Biol. 16:4604–4613; 1996.
39. Leek, R. D.; Landers, R. J.; Harris, A. L.; Lewis, C. E. Necrosis correlates with high vascular density and focal macrophage infiltration in invasive carcinoma of the breast. Br. J. Cancer 79:991–995; 1999.
40. Habeck, M. Wielding more power over angiogenesis. Mol. Med. Today 6:138–139; 2000.
41. Schwartsburd, P. M. Chronic inflammation as inductor of pro-cancer microenvironment: Pathogenesis of dysregulated feedback control. Cancer Metastasis Rev. 22:95–102; 2003.
42. Weiss, S. J. Tissue destruction by neutrophils. N. Engl. J. Med. 320:365–376; 1989.
43. Shanley, T. P.; Warner, R. L.; Ward, P. A. The role of cytokines and adhesion molecules in the development of inflammatory injury. Mol. Med. Today 1:40–45; 1995.